**LETTER**

# Theoretical investigation of two-dimensional sub-wavelength structures fabricated by multi-beam surface plasmon interference lithography

View the article online for updates and enhancements.

# Theoretical investigation of two-dimensional sub-wavelength structures fabricated by multi-beam surface plasmon interference lithography

Xiangxian Wang[1(a)], Tianxu Jia[1], Yaqian Ren[1], Yingwen Su[1], Zhenyu Chen[1], Yunping Qi[2] (ID)
and Xiaolei Wen[3]

[1] *School of Science, Lanzhou University of Technology - Lanzhou 730050, China*
[2] *College of Physics and Electronic Engineering, Northwest Normal University - Lanzhou 730070, China*
[3] *Center for Micro- and Nanoscale Research and Fabrication, University of Science and Technology of China Hefei 230026, China*

**Abstract** – In this study, multi-beam surface plasmon (SP) interference lithography was theoretically proposed and demonstrated to fabricate periodic two-dimensional sub-wavelength structures. The lithography structures were based on an attenuated total reflection prism used to excite the SPs using a 442 nm laser. Circular lattices with periods of 166 and 288 nm were successfully obtained via three- and six-beam SP interference lithography, respectively; these lattices exhibited an identical feature size of 96 nm. Square dot arrays with a 177 nm period and 88.5 nm spot size were obtained by four-beam SP interference lithography. The proposed lithography technology has a simple structure and is economical; further, it may provide an effective method for the fabrication of two-dimensional sub-wavelength structures.

**Introduction.** – With the advent of nanotechnologies, the properties of nanoscale structures have played a significant role in improving the performance of nanostructures in the fields of chemistry [1,2], materials science [3,4], and physics [5–8]. Many nanomanufacturing technologies have been developed for this purpose. Lithography is an effective technique for the fabrication of periodic nanostructures. The resolution of photolithography is generally affected by the diffraction limit of light. Therefore, a relatively short-wavelength light source and corresponding photoresist are generally used to obtain high-resolution nanostructures. Several lithography techniques have been proposed for nanofabrication purposes to achieve a high resolution. For example, immersion lithography [9] may be used to reduce the period of the resulting structure by improving the refractive index. Extreme ultraviolet lithography [10] and X-ray lithography [11] have improved the resolution of the resulting structures by shortening the wavelength. Sub-wavelength structures have attracted considerable attention because of their potential use in the design of desired optical properties and unique behaviors. However, it is expensive and difficult to use these techniques to achieve sub-wavelength structures.

Near-field technology [12] has been investigated to overcome the diffraction limit for nanofabrication processes. Evanescent-wave interference lithography [13] is a low-cost process for fabricating nanoscale structures. However, the optical intensity in the recording medium of this process is highly attenuated owing to the exponential decay of the evanescent waves. This technique provides a high resolution but is controlled by a short exposure depth and low transmission. Surface plasmon (SP) resonance phenomena, which have been widely used in surface-enhanced Raman scattering [14,15], sensing [16,17], and solar absorbers [18–20], can effectively address the above problem. SPs on a metal surface can significantly enhance light transmission and provide a novel method of near-field optical lithography that extends beyond the diffraction limit. SP-assisted nanoscale lithography, which is based on local field enhancement, has been demonstrated in recent years. Numerous researchers have theoretically and experimentally reported SP lithography methods based on grating coupling [21–24] and prism coupling [25–27], while the latter method has the advantage of being maskless. Sreekanth *et al.* generated one-dimensional grating

(a)E-mail: wangxx869@lut.edu.cn (corresponding author)

features with a 156 nm period by employing two-beam SP [28] and two-dimensional (2D) dot array patterns with a 175 nm period by utilizing four-beam SP [29] with an excitation wavelength of 364 nm. However, the use of additional beams and other abundant lattice morphologies have not been studied, and the theoretical simulations have not been described in detail. Guo *et al.* [25] provided an enhanced Kretschmann structure to obtain a desired nanoscale feature size by adding a PMMA dielectric layer. However, this study only focused on the fabrication of one-dimensional grating structures.

In this context, to overcome the above deficiencies and provide a prospective method for the above-described application, we present a multi-beam SP interference lithography system based on attenuated total reflection (ATR), which can fabricate periodic 2D sub-wavelength structures beyond the diffraction limits. A 442 nm laser is used as the excitation source for the SPs. Circular lattices with a feature size of 96 nm and 166 and 288 nm periods are successfully obtained via three- and six-beam SP interference lithography, respectively. Square dot arrays with a 177 nm period and 88.5 nm spot size can be obtained using four-beam SP interference lithography.

**Theoretical analysis of multi-beam surface plasmon interference lithography.** – Figure 1 shows schematics of multi-beam SP interference lithography setup. The $XOY$ plane is the interface of the silver (Ag) film and photoresist, and the $Z$-direction is perpendicular to the interface with the positive direction oriented toward the metal. Figure 1(a) shows a schematic of the SP interference lithography technique based on prism coupling. The Ag film is evaporated on the bottom of the prism, and an 80 nm photoresist is coated on the glass substrate. In the actual experiment, matching oil with the same refractive index as that of photoresist is often used to connect a metal and photoresist. This structure uses contact exposure. Figure 1(b) shows a schematic of the three-beam SP interference lithography technique. The incident lasers are uniformly distributed with a 120° azimuth angle and irradiated into the prism. Figure 1(c) depicts the four-beam SP interference lithography configuration; four-beam incident lasers irradiating into the prism are evenly distributed in space, and the azimuth angle of adjacent beams remains at 90°. Figure 1(d) is the six-beam SP interference lithography configuration, in which six-beam incident lasers are distributed evenly and the azimuth angle of adjacent beams is 60°, which irradiate into the top-cut hexagonal prism.

The dispersion relation for SPs between the photoresist and Ag film is described as follows [26]:

$$k_{sp} = k_0 \sqrt{\frac{\varepsilon_1 \varepsilon_2}{\varepsilon_1 + \varepsilon_2}}, \qquad (1)$$

where $k_{sp}$ is the wave vector of the SPs, $k_0$ represents the wave vector of the laser in vacuum, $\varepsilon_1$ is the complex permittivity of the Ag film, and $\varepsilon_2$ is the dielectric
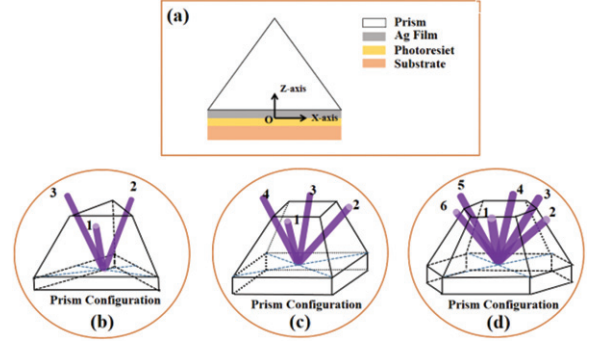


Fig. 1: Schematics of the multi-beam SP interference lithograph configuration: (a) prism coupling, (b) three-beam SP, (c) four-beam SP, and (d) six-beam SP.

constant of the photoresist. For prism coupling, the SPs can be effectively excited when the following equation is satisfied [25]:

$$k_0 \sqrt{\varepsilon_0} \sin \theta_{sp} = k_{sp}, \qquad (2)$$

where $\varepsilon_0$ is the dielectric constant of the prism and $\theta_{sp}$ is the resonance angle. The magnetic field $H_n$ of the SPs in the photoresist layer can be expressed as follows:

$$\begin{aligned} \vec{H}_n = t^p_{012} \cdot H_0 \cdot \exp[i(\cos\phi_n \cdot k_{sp} \cdot \vec{x} \\ + \sin\phi_n \cdot k_{sp} \cdot \vec{y} - k_z \cdot \vec{z} - \omega t)], \end{aligned} \qquad (3)$$

where $H_0$ is the magnetic field intensity of the incident beam, $t^p_{012}$ represents the maximum field enhancement [26], $\phi$ is the azimuth angle, $k_z$ is the wave vector parallel to the $Z$-axis in the photoresist (defined by the equation $k_z^2 = \varepsilon_2 k_0^2 - k_{sp}^2$), $\omega$ is the frequency, and $t$ is the time. The field intensity ($I$) distribution in the photoresist can be expressed as follows [26]:

$$I = \left(\vec{H}_1 + \cdots + \vec{H}_n\right)\left(\vec{H}_1^* + \cdots + \vec{H}_n^*\right). \qquad (4)$$

**Simulation results and discussion.** – In the simulation, we chose a 442 nm laser as the excitation source for the SPs. For the convenience of the calculations, $H_0$ was assumed to be one. The refractive indices of the prism, photoresist, and substrate were 1.8219 (N-LAF36), 1.53 [30], and 1.52 (BK7), respectively. An Ag film was used as the metal film, and the complex dielectric constant at 442 nm was $-8.9170+0.232i$ [30]. Figure 2 shows the reflectance spectra obtained for different Ag thicknesses, from which we can note an optimal thickness of 44 nm and a corresponding resonance angle of 76.19°. Other reflection spectra have low reflectivity compared with that of the reflection spectra of 44 nm Ag film. Although field intensity will be decreased, they still meet the requirements of SP interference lithography.
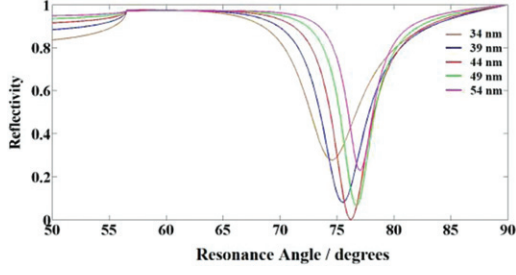
Fig. 2: Reflectance spectra of varied Ag thicknesses.

Next, we studied the arrangement and period of the 2D sub-wavelength structures using multi-beam SP interference lithography. Figure 3(a) displays the three-dimensional (3D) optical field distribution (OFD) while fig. 3(b) illustrates the 2D OFD with $Z = 0$ nm obtained by three-beam SP interference lithography. 2D sub-wavelength circular lattices, which are quasi-hexagonally close-packed, can be fabricated using a negative photoresist. Each circular dot is uniformly surrounded by six circular dots with the same radius as that of the central dot; these six dots form an equilateral hexagon with a side length of 166 nm. Honeycomb circular arrays can be fabricated using a positive photoresist. Figures 3(c) and (d) depict the 3D and 2D OFDs with $Z = 0$ nm, respectively, obtained by four-beam SP interference lithography. 2D sub-wavelength square lattices can be fabricated using a negative photoresist. A square lattice with a 177 nm side length was formed by the four adjacent dots. The period was $\sqrt{2}$ times that obtained via re-exposure after rotating the sample by 90° following the double-beam exposure [26]. Figures 3(e) and (f) present the 3D and 2D ($Z = 0$ nm) OFDs obtained by six-beam SP interference lithography, respectively. The lattices demonstrated the same arrangement of being quasi-hexagonally close-packed as was obtained using three-beam SP interference lithography, but the former exhibited a larger period with a value of 288 nm. Honeycomb circular arrays can be fabricated in both modes for a positive photoresist, but the sub-wavelength structures obtained using six-beam SP interference lithography have sharper edges.

The feature size was further investigated. Figures 4(a), (c), and (e) display the simulation diagrams of the $YOZ$ plane obtained using three-, four-, and six-beam SP interference lithography processes, respectively. Figures 4(b), (d), and (f) illustrate the intensity curves obtained with $Z = 0$ nm corresponding to the conditions of figs. 4(a), (c), and (e), respectively. The circular lattices exhibited a feature size of 96 nm as obtained using three-beam SP interference lithography. Dot arrays with an 88.5 nm feature size were obtained by four-beam SP interference lithography. Six-beam SP interference lithography resulted in the same feature size of 96 nm as that obtained using three-beam SP interference lithography. Considering the results of this experiment, the quality of the interference pattern
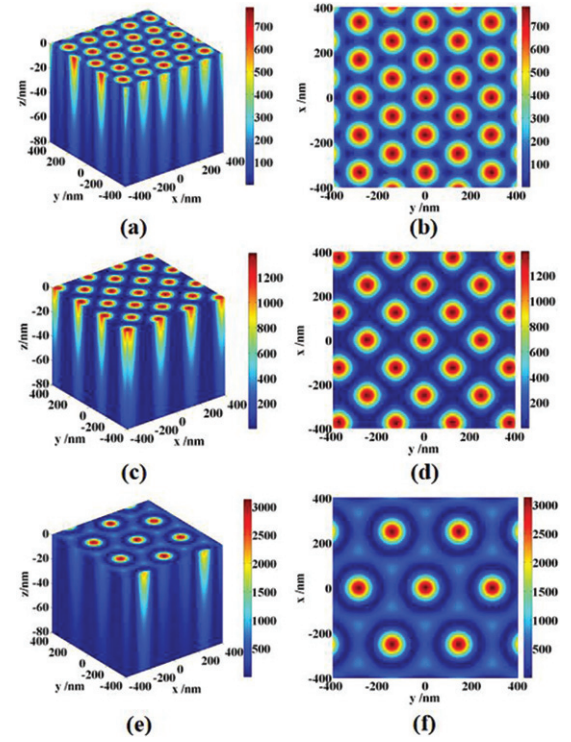


Fig. 3: OFDs of multi-beam SP interference lithography: (a) and (b): circular lattices written by three-beam SP lithography; (c) and (d): square dot arrays written by four-beam SP lithography; (e) and (f): circular lattices written by six-beam SP lithography.
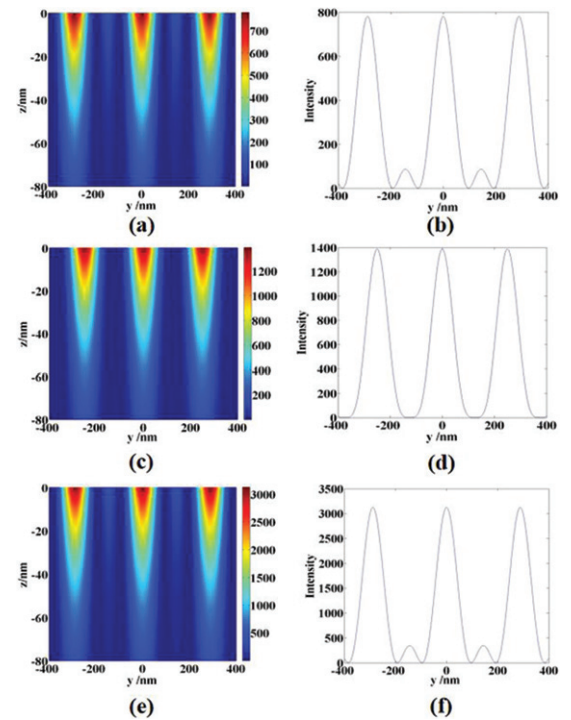


Fig. 4: OFDs of (a) three-, (c) four-, and (e) six-beam SP interference lithography on the $YOZ$ plane. Panels (b), (d), and (f) are the intensity curves with $Z = 0$ nm corresponding to (a), (c), and (e), respectively.

is normally dependent upon the contrast and OFD. The contrast ($V$) of the interference pattern can be described as $V = (I_{max} - I_{min})/(I_{max} + I_{min})$, where $I_{max}$ and $I_{min}$ are the maximum and minimum intensities in one period, respectively. For the above 2D sub-wavelength structures, $I_{min}$ generally approaches zero; therefore, the contrast is equivalent to one.

According to the above calculation and discussion, both negative and positive photoresists can be used for the proposed SP interference lithography, and only opposite patterns can be obtained. Each calculated contrast in this study is close to one, which is sufficient to achieve high-quality sub-wavelength structure for the photoresist. Compared with other lithography methods, for example, laser interference and optical projection lithography, the advantages of this method are that it is maskless, is low-cost, and overcomes the diffraction limit. Additionally, its structures and shapes are more regular compared with those of chemical methods. The proposed method still requires an ATR prism with a high refractive index. Moreover, the complexity of the optical path increases with the addition of beams.

In this paper, we only discuss Ag as a metal film and the photoresist of a refractive index of 1.53 as a resist layer. In the practical experiment, if the refractive index of photoresist is changed, the $\theta_{sp}$ and $k_{sp}$ of the SPs will change. Consequently, 2D sub-wavelength structures of different periods and feature sizes are obtained, but their morphologies are the same as those calculated above. In addition, other metals, such as aluminum, can also be used as the metal layer. Under this condition, a 325 nm laser is used as the excitation light source. This will yield smaller feature sizes and periods, but shapes and arrangements will remain the same as those in the above simulation. Using a specific combination of photoresist and metal, 2D sub-wavelength structures with different feature sizes and periods are obtained, and their shapes and arrangements are consistent with those calculated in this study. Thus, the lithography method proposed in this paper is universal. In actual lithography, photoresist, metal film, and excitation light source can be selected according to actual demands.

**Conclusions.** – We provided a theoretical presentation of a multi-beam SP interference lithography system for fabricating 2D sub-wavelength structures. This method is based on an ATR prism that is used to excite SPs using a 442 nm laser, which is a simple and low-cost system. Different sub-wavelength structures were obtained by changing the number of beams. Circular lattices with periods of 166 and 288 nm were successfully obtained via three- and six-beam SP interference lithography, respectively; these lattices exhibited the same feature size of 96 nm. Square dot arrays with a 177 nm period and 88.5 nm feature size were achieved via four-beam SP interference lithography. This lithography technique is expected to provide an effective method for the fabrication of 2D sub-wavelength structures. The proposed method is promising for lithography at a high contrast and resolution that can provide potential applications in various areas, such as photonic crystals, sensing, surface-enhanced Raman scattering, and waveguide fabrications.

$$* * *$$

*Data availability statement*: The data that support the findings of this study are available upon reasonable request from the authors.

REFERENCES

[1] Gao H., Zhao X., Zhang H., Chen J., Wang S. and Yang H., *J. Electron. Mater.*, **49** (2020) 5248.

[2] Guan S., Li R., Sun X., Xian T. and Yang H., *Mater. Technol.*, **36** (2020) 603.

[3] Liu G., Chen J., Pan P. and Liu Z., *IEEE J. Sel. Top. Quantum Electron.*, **25** (2019) 4600507.

[4] Jiang L., Yuan C., Li Z., Su J. and Pan M., *Diam. Relat. Mater.*, **111** (2021) 108227.

[5] Liu C., Yang L., Liu Q., Wang F., Sun Z., Sun T., Mu H. and Chu P., *Plasmonics*, **13** (2018) 779.

[6] Liu C., Wang J., Wang F., Su W., Yang L., Lv J., Fu G., Li X., Liu Q., Sun T. and Chu P., *Opt. Commun.*, **464** (2020) 125496.

[7] Qi Y., Zhang B., Ding J., Zhang T., Wang X. and Yi Z., *Chin. Phys. B*, **30** (2021) 024211.

[8] Wang X., Zhu J., Xu Y., Qi Y., Zhang L., Yang H. and Yi Z., *Chin. Phys. B*, **30** (2021) 024207.

[9] Jakkinapalli A., Bhaskar A. and Wen S. B., *J. Micromech. Microeng.*, **30** (2020) 125014.

[10] Kim S., *J. Nanosci. Nanotechnol.*, **21** (2021) 4466.

[11] Maldonado J. R. and Peckerar M., *Microelectron. Eng.*, **161** (2016) 87.

[12] Fan H. and Richard B., *Adv. Opt. Mater.*, **7** (2019) 1801653.

[13] Masui S., Torii Y., Michihata M., Takamasu K. and Takahashi S., *Opt. Express*, **27** (2019) 31522.

[14] Wang X., Wu Y., Wen X., Zhu J., Bai X., Qi Y. and Yang H., *Opt. Quantum Electron.*, **52** (2020) 238.

[15] Wu Y., Wang X., Bai X., Zhu J. and Qi Y., *Phys. Lett. A*, **384** (2020) 126544.

[16] Chen J., Nie H., Peng C., Qi S., Tang C., Zhang Y., Wang L. and Park G., *J. Lightwave Technol.*, **36** (2018) 3481.

[17] Wang X., Zhu J., Tong H., Yang X., Wu X., Pang Z., Yang H. and Qi Y., *Chin. Phys. B*, **28** (2019) 044201.

[18] Liu Z., Tang P., Liu X., Yi Z., Liu G., Wang Y. and Liu M., *Nanotechnology*, **30** (2019) 305203.

[19] Zhang Y., Yi Z., Wang X., Chu P., Yao W., Zhou Z., Cheng S., Liu Z., Wu P., Pan M. and Yi Y., *Phys. E*, **127** (2021) 114526.

[20] Zhang B., Qi Y., Zhang T., Zhang Y. and Yi Z., *Results Phys.*, **26** (2021) 104233.

[21] Kong W., Lou Y., Zhao C., Liu L., Gao P., Pu M., Wang C. and Luo X., *ACS Appl. Nano Mater.*, **2** (2019) 489.

[22] Liu H., Kong W., Zhu Q., Zheng Y., Shen K., Zhang J. and Lu H., *J. Phys. D: Appl. Phys.*, **53** (2020) 135103.

[23] Wang Q., Zheng Y., Yu C., Chen X., Wang E., Long S., Zhu H., Gao S. and Cao J., *Plasmonics*, **15** (2020) 1639.

[24] Bourke L. and Blaikie R., *J. Opt. A*, **19** (2017) 095003.

[25] Guo X., Dong Q., Shi R., Li S. and Du J., *Microelectron. Eng.*, **105** (2013) 103.

[26] Wang X., Pang Z., Tong H., Wu X., Bai X., Yang H., Wen X. and Qi Y., *Results Phys.*, **12** (2019) 732.

[27] Kusaka K., Kurosawa H., Ohno S., Sakaki Y., Nakayama K., Moritake Y. and Ishihara T., *Opt. Express*, **22** (2014) 18748.

[28] Sreekanth K. V. and Murukeshan V. M., *J. Micro/Nanolithogr. MEMS MOEMS*, **9** (2010) 023007.

[29] Sreekanth K. V. and Murukeshan V. M., *J. Vac. Sci. Technol., B*, **28** (2010) 128.

[30] Guo X., Du J., Guo Y. and Yao J., *Opt. Lett.*, **31** (2006) 2613.